Analytical depth-dose curves in radiotherapy with hadrons

Author: Marta Marín de Castro
Facultat de Física, Universitat de Barcelona, Diagonal 645, 08028 Barcelona, Spain

Advisor: José María Fernández-Varea
(Dated: 14/01/2024)

Abstract: Hadrons are increasingly used in external-beam radiotherapy owing mainly to their characteristic Bragg-peak depth-dose curves, which are suitable to treat deep-seated tumors. An analytical approach to this distribution, rather than relying on measured or numerically calculated data, offers several advantages. This report aims to provide an analytical model for proton ($^1H^+$) and alpha particle ($^4He^{2+}$) beams traversing liquid water, as surrogate of human tissue. The model is based on the following premises: (i) the particle energy loss is described beyond the continuous-slowing-down approximation following Bethe–Bloch function, (ii) the range-energy dependency follows a power-law relationship, (iii) the particle fluence decreases linearly with depth due to nonelastic nuclear interactions and (iv) the range straggling distribution can be approximated by a Gaussian.

I. INTRODUCTION

Hadron radiotherapy, encompassing treatments with protons and carbon ions, began gaining attention for its potential in cancer treatment around the latter part of the 20th century [1]. However, its widespread recognition and growing popularity as an advanced form of radiotherapy have notably evolved in more recent years, particularly from the early 2000s onward, marking a promising usage of hadron therapy in modern oncology.

The rise in prominence of hadron-based therapies stems from by their distinct physical and radio-biological characteristics. Starting by their main advantage, hadron beams exhibit a characteristic depth-dose profile curve commonly referred to as the Bragg peak due to its distinctive shape. This feature not only allows accurate and optimal energy delivery, but also access to greater depths within the patient in comparison to conventional photon or electron radiotherapy, which predominantly deposit the majority of their energy close to the tissue's entry point within the patient. This well-defined range of irradiation together with a small lateral beam spread minimizes the irradiation of healthy tissues surrounding the targeted area [2].

Concurrently, heavy charged particles, due to their high linear energy transfer (LET), possess an enhanced relative biological effectiveness (RBE), which characterize the damage induced to the cells. This makes them particularly advantageous for targeting radioresistant or hypoxic tumors where conventional treatments may be less effective. Hadrons also lack Bremsstrahlung emission, and this favours a more concentrated deposition of energy in the targeted ill tissue [3].

Taking into account the outlined advantages, it is understandable that the use of high-energy proton beams in radiotherapy has become a topic of increasing interest and research. Alpha particles have recently started being studied because they exhibit superior physical properties such as reduced lateral scattering and range straggling, as well as higher RBE and LET [4].

Our main objective is to review an analytical approximation for hadrons' Bragg curves as this would entail a better understanding of advantages hadron therapy exhibit and faster dose calculation algorithms in treatment planning systems.

The report is organized as follows: Section II focuses on the physics behind monoenergetic parallel beams travelling through matter and the magnitudes used to characterize this process which help build a semi-empirical model, Section III describes the analytical model to ultimately obtain the depth-dose curve (longitudinal dose profile) and, finally, section IV concludes the paper.

II. SEMI-EMPIRICAL MODEL

When traversing biological tissues, charged particles generally dissipate energy primarily through electromagnetic inelastic interactions with target electrons. As these particles decelerate, the energy loss rate escalates, especially at greater depths. This phenomenon correlates with a progressive elevation in LET, culminating in the distinctive Bragg peak profile [3].

Charged particles lose kinetic energy stochastically in small amounts, which is called continuous-slowing-down approximation (CSDA). This energy loss is well characterized by the stopping power, defined as the energy loss per unit path length s, due to inelastic collisions with the electrons of the medium. The mass electronic stopping power is predicted by the relativistic Bethe–Bloch formula based on the Born approximation [5]:

$$\frac{S_{el}}{\rho} \equiv \frac{1}{\rho}\left(-\frac{dE}{ds}\right) = C_0\,\frac{Z_1^2}{\beta^2}\,\frac{Z_2}{A_2}\,L_0(\beta), \tag{1}$$

where C_0=0.307 075 MeV cm^2/g, Z_1 is the charge of the projectile, Z_2, A_2 and ρ represent the atomic number, mass number and mass density of liquid water as the stopping material. In turn, L_0 is the Bethe stopping number

$$L_0 = \ln\left(\frac{2m_e c^2\,\beta^2\gamma^2}{I}\right) - \beta^2 - \frac{C}{Z_2} - \frac{\delta}{2}, \tag{2}$$

where $I = 78$ eV is the mean excitation energy of liquid water.

For specific energies E/M (M is the mass of the projectile) commonly employed in radiotherapy, which range from approximately 1 to 200 MeV/u so as to reach depths up to around 25 cm, the inclusion of the shell correction C/Z_2 and density-effect correction δ improves the agreement with tabulated values, as depicted for protons in Fig. 7 in the Appendix. The former, C/Z_2, accounts for the internal motion of the target electrons because they are not stationary. Due to the simplifications made in the derivation of Eq. (1), when the projectile's kinetic energy is low, the values provided by the formula deviate from experimental values. This difference determines the shell correction [6], which is appreciable at low energies. The latter, δ, accommodates the polarization of atoms in a dense medium as charged particles traverse through it. This phenomenon, relevant at relativistic energies, occurs as atoms farther from the path of a charged particle experience a diminished Coulomb field i.e. the stopping power is reduced [5].

Therefore, these two corrections will be incorporated into the semi-empirical model, aiming to align the analytical model as close with reality as possible. Implementation of these adjustments yields results in Fig. 1.

Eqs. (1) and (2) omit other low- and high-energy corrections, whose correspondent effects are not significant within the energy range of interest. Fig. 8 included in the Appendix illustrates the limitations of the formula without correction: it is inaccurate for energies below 1 MeV/u and above 1000 MeV/u.

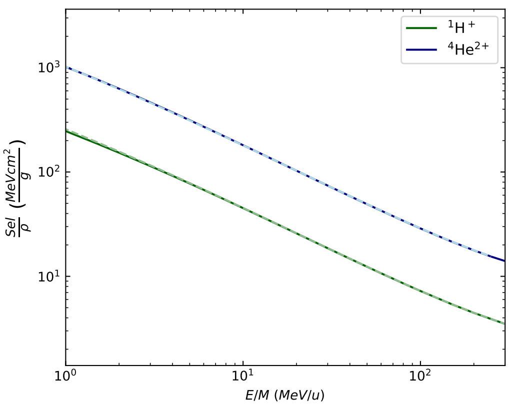

FIG. 1: Mass electronic stopping power as a function of specific energy for $^1H^+$ and $^4He^{2+}$ beams in liquid water obtained with the Bethe–Bloch formula (continuous curves) and tabulated values from ICRU Report 90 [5] (dashed curves).

The CSDA range r_0 is the depth at which the ions of the beam come to rest, defining the average distance of penetration within a given medium. It is computed as follows

$$\rho r_0 = \int_0^E \frac{1}{S_{el}(E')/\rho}\, dE'. \tag{3}$$

Fig. 2 illustrates that, for energies of interest in radiotherapy treatments, the CSDA range exhibits a power-law dependence on depth. This observation constitutes the starting point for the analytical model described below.

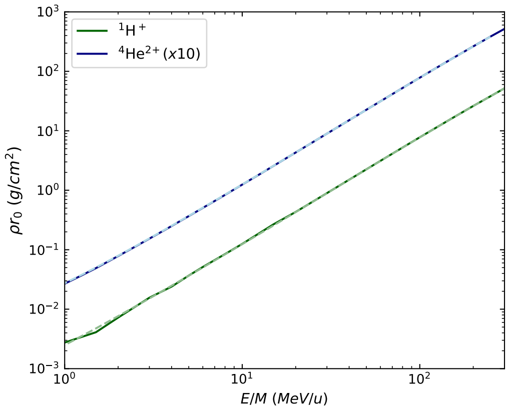

FIG. 2: Mass CSDA range as a function of specific energy for $^1H^+$ and $^4He^{2+}$ beams in liquid water obtained with the Bethe Bloch formula (continuous curves) and tabulated values from ICRU Report 90 (dashed curves). Note that data for $^4He^{2+}$ ions are multiplied by 10.

When a beam of hadrons traverses matter, some of the ions are lost from the beam because of nuclear interactions with the atomic nuclei of the target material. The energy fluence as a function of depth z in the material, $\Psi(z) = \Phi(z)\,E(z)$, must reflect that both the particle fluence (number of particles crossing a unit area), $\Phi(z)$, and the beam energy, $E(z)$, depend on z. Hence, the absorbed dose for mono-energetic beams takes the form [7]

$$\hat{D}(z) = -\frac{1}{\rho}\frac{d\Psi(z)}{dz} = -\frac{1}{\rho}\left[\Phi(z)\,\frac{dE(z)}{dz} + \gamma\,\frac{d\Phi(z)}{dz}\,E(z)\right]. \tag{4}$$

The first term describes how the beam loses energy with increasing depth, i.e. the stopping power of Eq. (1), whereas the second one contains the reduction of particle fluence with depth, i.e. the beam attenuation due to nuclear reactions. γ is the fraction of the energy released in the nonelastic nuclear interactions that is absorbed locally; a reasonable value for this parameter is $\gamma = 0.6$.

The particle fluence decreases according to the Beer–Lambert law [8]

$$\Phi(z) = \Phi_0 \exp\left(-\frac{\mu}{\rho}\rho z\right), \tag{5}$$

where Φ_0 is the fluence of the beam at $z = 0$ and μ/ρ is the mass attenuation coefficient that can be described as

$$\frac{\mu}{\rho} = \frac{N_A\, \sigma_R}{\mathcal{M}}, \tag{6}$$

where N_A is the Avogadro constant, $\mathcal{M} = 18.015$ g/mol is the molar mass of H_2O, and σ_R is the reaction cross section that has been taken as constant $\sigma_R(E_0)$ and whose calculation and behavior can be found in the Appendix, Eq. (16) and Fig. 10.

III. BORTFELD'S ANALYTICAL MODEL

As shown in Fig. 2, the correlation between the energy of the incident beam E_0 and the distance traveled within the medium r_0 is estimated to be linear, so a power-law relationship can be defined following Bortfeld [7]:

$$r_0 = \alpha\, E^p. \tag{7}$$

To determine the adjustable parameters α and p, the Levenberg–Marquardt minimization algorithm [9] is employed to fit the most recent tables of CSDA ranges as a function of initial beam energy from ICRU Report 90. Table I lists the parameters obtained for protons and alpha particle for the energy interval of 5–200 MeV/u. Old tabulated values for protons from ICRU Report 49 [10] have also been fitted to reproduce Bortfeld's approach, which was also based on the now obsolete value of $I =$ 75 eV for liquid water. The respective fitting figures can be found in the Appendix, Fig. 9. The acquisition of these parameters enables the ongoing development of the model.

TABLE I: Fitting parameters α and p in Eq. (7) using data from ICRU Report 90 for protons and alpha particles. For $^1H^+$ beams, parameters obtained Bortfeld's fitting method with ICRU 49 tabulated values[7] have also been included.

Ion	Data	α	p
$^1H^+$	ICRU 49, Bortfeld	2.2×10^{-3}	1.77
$^1H^+$	ICRU 90	2.360×10^{-3}	1.758
$^4He^{2+}$	ICRU 90	2.147×10^{-4}	1.752

Understanding the evolution of the beam energy with depth, $E(z)$, based on its initial energy E_0, is important for both therapeutic and illustrative objectives as it facilitates the assessment of tumor treatment concerning its depth within the patient. Analogous to (7), the relationship between range and energy can be expressed as $r_0 - z = \alpha\, E^p(z)$, from which the energy of the beam as a function of depth is directly derived

$$E(z) = \frac{1}{\alpha^{1/p}}\,(r_0 - z)^{1/p}. \tag{8}$$

This formula effectively replicates the characteristics of the semi-empirical model concerning the variation of energy with depth, as seen in Fig. 3 for protons and alpha particles. It is apparent that alpha particles require a greater initial kinetic energy compared to protons to attain identical depths.

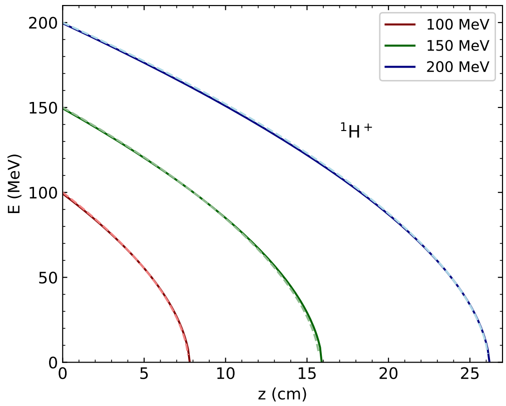

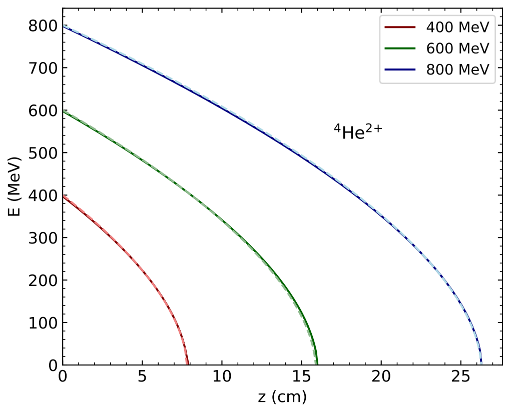

FIG. 3: Energy of $^1H^+$ (top) and $^4He^{2+}$ (bottom) beams as a function of depth for initial specific energies of 100, 150 and 200 MeV/u. The continuous and dashed curves were calculated with the analytical and semi-empirical models, respectively.

The mass stopping power is now approximated as

$$S(z) = \frac{1}{p\alpha^{1/p}}\,(r_0 - z)^{1/p-1}. \tag{9}$$

Janni [11] tabulated the probability, denoted as P, characterizing these nonelastic nuclear interactions relative to the residual range, $r_0 - z$. Lee et al. [12] established a proportional relationship for the fluence as a function of depth,

$$\Phi(z) \propto \frac{1}{1 - P(r_0 - z)} \approx 1 + \beta\,(r_0 - z), \tag{10}$$

with β= 0.012 cm^{-1} as the slope parameter for protons. The fluence normalized to the incident fluence is then

$$\Phi(z) = \Phi_0\, \frac{1 + \beta\,(r_0 - z)}{1 + \beta\, r_0}. \tag{11}$$

As Fig. 4 displays, the fluence predicted by Eq. (11) is in good agreement with the semi-empirical model for beams of 200 MeV/u protons and alpha particles. For the latter, the best agreement with the empirical model was found for a slope parameter $\beta = 0.026$ cm^{-1}.

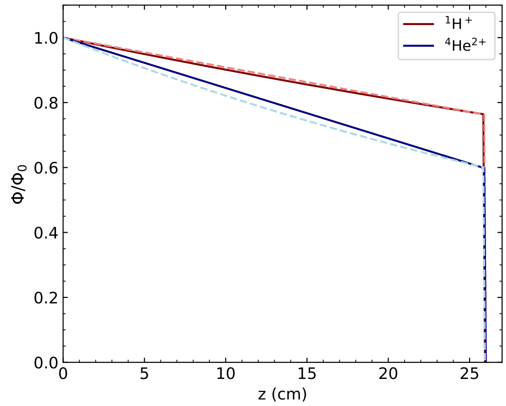

FIG. 4: Normalized fluence as a function of depth obtained by the semi-empirical (dashed lines) and analytical (continuous curves) models for 200 MeV/u ^{1}H$^+$ and ^{4}He^{2+} beams.

The normalized fluence has been computed for two greater initial energies reaching depths of 7 and 16 cm. Results for protons and alpha particles can be found in Fig. 5. There is a greater loss of particle fluence for alpha particles owing to the larger nuclear reaction cross section (see the Appendix).

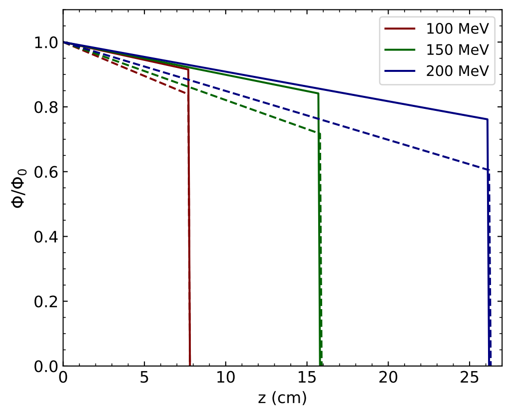

FIG. 5: Normalized fluence as a function of depth. Initial beam energies of 100, 150 and 200 MeV/u have been considered for ^{1}H$^+$ (continuous curves) and ^{4}He^{2+} (dashed curves) beams.

The depth-dose distribution, excluding the effect of range straggling, can be readily computed by inserting Eqs. (8), (9) and (11) into Eq. (4),

$$\frac{\hat{D}(z)}{\Phi_0} = \begin{cases} \Phi_0 \, \frac{(r_0-z)^{1/p-1}+(\beta+\gamma\beta p)(r_0-z)^{1/p}}{\rho p \alpha^{1/p}(1+\beta r_0)} & \text{if } z < r_0, \\ 0 & \text{if } z \geq r_0. \end{cases} \tag{12}$$

As mentioned above, the CSDA neglects fluctuations linked to the energy loss in inelastic collisions, resulting in a well-defined $E(z)$ curve. Consequently, all particles are expected to halt at exactly the CSDA range r_0, see Fig. 3. In reality, due to the statistical fluctuations inherent in energy-loss interactions, ions come to rest across a range of depths, a phenomenon referred to as range straggling [1]. Note that nuclear reactions generate a spectrum of particles and secondary target fragments, with varying energy and LET, that contribute as well to the absorbed dose beyond r_0 [3]. This range distribution closely resembles a Gaussian distribution, with its variance determined by

$$\sigma_z^2 = \alpha' \, \frac{p^2 \alpha^{2/p}}{3-2/p} \, r_0^{3-2/p}, \tag{13}$$

with $\alpha' = 0.087$ MeV^2/cm. Therefore, the effect of range straggling is introduced by convolving the CSDA absorbed dose $\hat{D}(z)$ with the Gaussian distribution

$$G(z;\overline{z},\sigma_z) = \frac{1}{\sqrt{2\pi\sigma_z^2}} \exp\left(-\frac{1}{2}\,\frac{(z-\overline{z})^2}{\sigma_z^2}\right), \tag{14}$$

which yields the sought longitudinal depth-dose profile

$$\frac{D(z)}{\Phi_0} = \int_0^{r_0+2\sigma_z} \frac{\hat{D}(\overline{z})}{\Phi_0} \, G(z;\overline{z},\sigma_z) \, d\overline{z}. \tag{15}$$

Observing Fig. 6, the introduction of range straggling indeed corrects the unphysical divergence of $\hat{D}(z)$ at the CSDA range. Comparing these figures, it is clear that the absorbed dose is greater for alpha particles. This asset, coupled with a narrower penumbra, a more linear trajectory, and a reduced nuclear fragmentation tail beyond the peak [13], makes alpha particles a good option for treating deeply situated tumors. This ultimately leads to a more predictable radiation delivery, enhancing control over the treatment's effects.

Lastly, the superposition of monoenergetic beams with different CSDA ranges, multiplied by suitable weights, results in a "spread-out Bragg peak" (SOBP) that achieves a nearly uniform absorbed dose in the tumor, aiming to treat every affected area thoroughly.

IV. CONCLUSIONS

Tested on protons and alpha particles for beam energies ranging from 1 to 200 MeV/u, the analytical model evaluated throughout this work has proven successful in reproducing semi-empirical values for magnitudes related to hadron energy loss when traversing matter. In

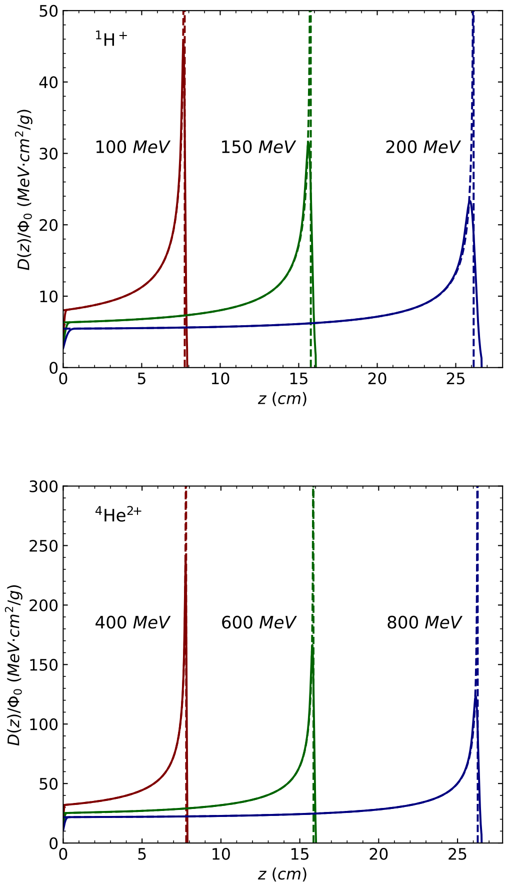

FIG. 6: Depth-dose curves with (continuous curves) and without (dashed curves) consideration of range straggling for 100, 150 and 200 MeV/u ^{1}H$^+$(top) and ^{4}He^{2+}(bottom) beams.

comparison to traditionally used particles, the resulting hadron depth-dose distribution allows to comprehend harons' ability to administer doses to be deeper and more accurate. This fact, coupled with other advantages, makes hadron-beam radiotherapy stand out as an advantageous cancer treatment method. Specifically, alpha particles present a viable choice for radioresistant tumors due to their greater biological impact. This benefit makes them notably promising for future investigation.

Acknowledgments

I wish to express my sincere gratitude to my supervisor, José M. Fernández-Varea, for his unwavering guidance, support, and counsel throughout the development of this work. I would also like to state my sincere appreciation to my family and friends, who consistently inspire me with love, care and motivation.

[1] R.R. Wilson, Radiological use of fast protons. *Radiol.* **47**, 487 (1946).
[2] D. Schardt, T. Elsässer, D. Schulz-Ertner. Heavy-ion tumor therapy: Physical and riodiobiological benefits. *Rev. Mod. Phys.* **82**, 383 (2010).
[3] F. Tommasino, M. Durante. Proton Radiobiology. *Cancers* **7**, 353–381 (2015).
[4] A. Mairani et al. Roadmap: helium ion therapy. *Phys. Med. Biol.* **67**, 15TR02 (2022). *Int. J. Imaging Syst. Technol.* **6**, 1–128 (1995).
[5] S.M. Seltzer et al. ICRU Report 90: Key Data for Ionizing-Radiation Dosimetry: Measurement Standards and Applications. (ICRU, 2016).
[6] F. Salvat. Bethe stopping-power formula and its corrections. *Phys. Rev. A* **106**, 032809 (2022).
[7] T. Bortfeld. An analytical approximation of the Bragg curve for therapeutic proton beams. *Med. Phys.* **24**, 2024 (1997).
[8] M. Lazzeroni. Production of high quality ^{11}C beams for radiation treatment and accurate PET-CT dose delivery verification. (PhD Thesis, University of Stockholm, 2013).
[9] K. Levenberg, Un método para la solución de ciertos problemas no lineales en mínimos cuadrados. Trimestral de Matemática Aplicada 2, 164–168 (1944).
[10] International Commission on Radiation Units and Measurements, Bethesda, MD *ICRU Report 49: Stopping Powers and Ranges for Protons and Alpha Particles.* (ICRU, 1993).
[11] J.F. Janni. Proton range-energy tables, 1 keV-10 GeV. *At. Data Nucl. Data Tables* **27**, 147–339 (1982).
[12] M. Lee, A.E. Nahum, S. Webb. An empirical method to build up a model of proton dose distribution for a radiotherapy treatment planning package. *Phys. Med. Biol.* **38**, 989–998 (1993).
[13] J.W. Norbury et al. Are further cross section measurements necessary for space radiation protection or ion therapy applications? Helium projectiles. *Front. Phys.* **8**, 565954 (2020).
[14] S. Kox et al. Trends of total reaction cross sections for heavy ion collisions in the intermediate energy range. *Phys. Rev. C* **35**, 1678 (1987).

V. APPENDIX

Nuclear reaction cross section

The nuclear reaction cross section of hadron beams with oxygen $^{16}O^{+}$ is formulated following the semi-empirical model by Kox et al. [14]:

$$\sigma_R = \pi r_0^2 \left[A_P^{1/3} + A_T^{1/3} + S(A_P, A_T) - c(\epsilon) \right] \left(1 - \frac{V_B}{E_{CM}} \right), \quad (16)$$

where P and T stand for projectile and target, respectively, $r_0 = 1.1$ fm, $S(A_P, A_T)$ is the mass asymmetry function and $c(\epsilon)$ the transparency function. Below formulation of these magnitudes can be found.

$$S(A_P, A_T) = a \frac{A_P^{1/3} A_T^{1/3}}{A_P^{1/3} + A_T^{1/3}}, \quad (17)$$

with $a = 1.85$. The height of the Coulomb barrier is

$$V_B = \frac{Z_P Z_T e^2}{R_B} - b \left(\frac{1}{R_P} + \frac{1}{R_T} \right)^{-1}, \quad (18)$$

where $b = 1$ MeV/fm and the barrier position is given by

$$R_B = R_P + R_T + \Delta R, \quad (19)$$

with:

$$R_i = (1.12 fm) A_1^{1/3} - (0.94 fm) A^{-1/3}, \quad (20)$$

being $\Delta R = 3.2$ fm and $i = P, T$.

The non-relativistic kinetic energy in the center-of-mass frame is

$$E_{cm} = \left(\frac{1}{A_P} + \frac{1}{A_T} \right)^{-1}. \quad (21)$$

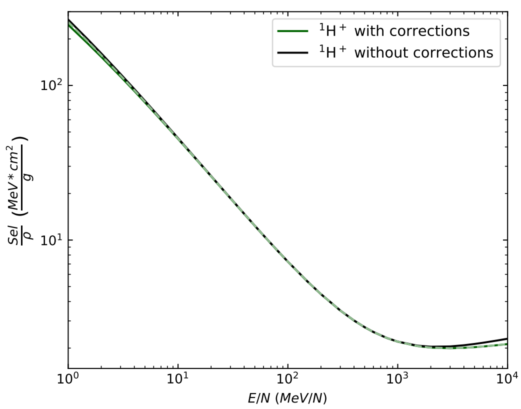

FIG. 7: Mass electronic stopping power as a function of energy per unit mass with and without including the shell and density-effect corrections. Studied for $^1H^+$ in liquid water. The dashed curves are the tabulated values from ICRU Report 90.

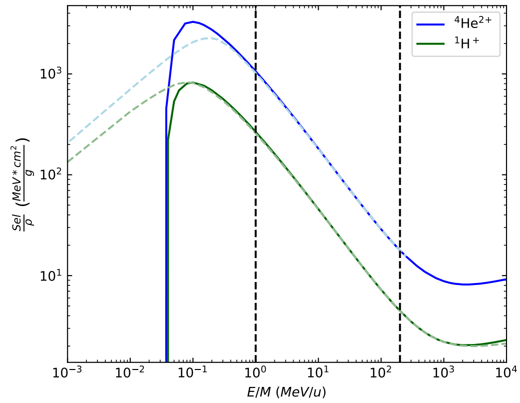

FIG. 8: Mass electronic stopping power as a function of energy per nucleon without including any corrections. Tested for $^1H^+$ and $^4He^{2+}$ beams in liquid water. Dashed line represents the tabulated values from ICRU Report 90. The energy range between the vertical dashed lines corresponds to that of concern in radiotherapy.

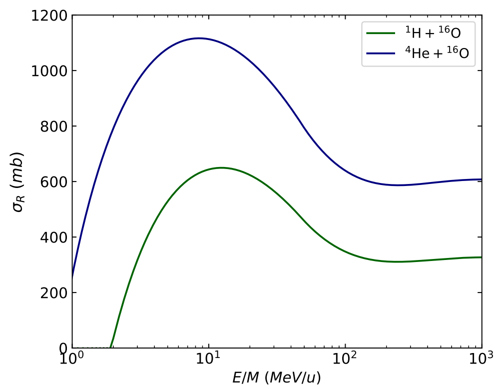

FIG. 10: Reaction cross section as a function of specific energy for ^1H and ^4He nuclei as projectiles and ^{16}O nuclei as target.

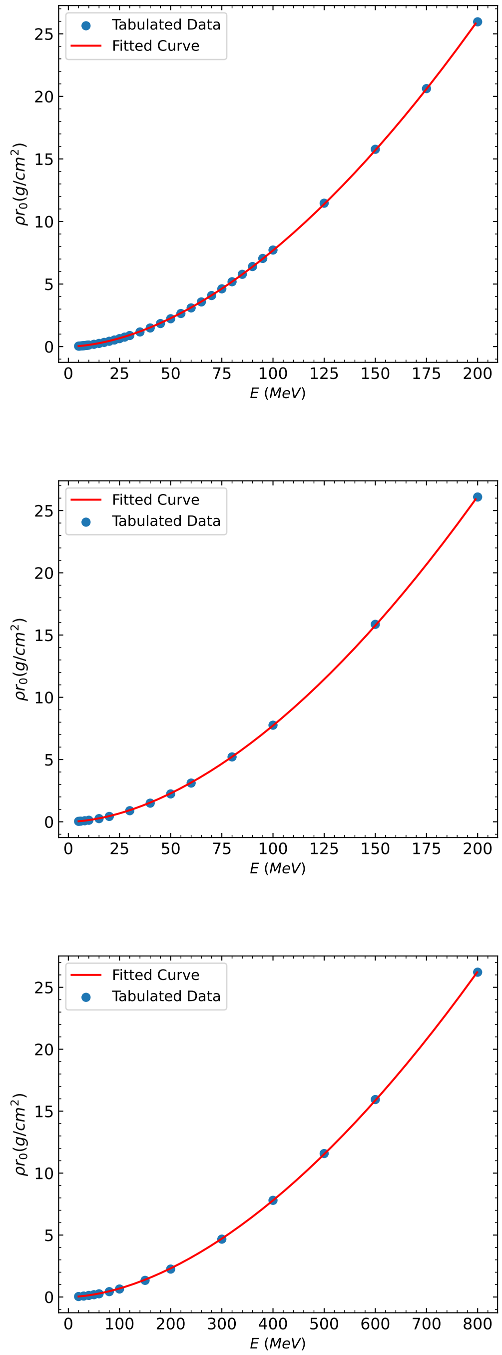

FIG. 9: Fitting as a power relationship tabulated values for CSDA range r_0 and initial energy E_0 of $^1H^+$ beams from ICRU Report 49 (top) and ICRU Report 90 (middle) and of $^4He^{2+}$ beams from ICRU Report 90 (bottom).